Magnetic properties of $CeCu_2$ tested by muon-spin rotation and relaxation

2004 J. Phys.: Condens. Matter 16 2421

(http://iopscience.iop.org/0953-8984/16/13/020)

INSTITUTE OF PHYSICS PUBLISHING JOURNAL OF PHYSICS: CONDENSED MATTER

J. Phys.: Condens. Matter **16** (2004) 2421–2436 PII: S0953-8984(04)75897-X

Magnetic properties of $CeCu_2$ tested by muon-spin rotation and relaxation

F N Gygax[1,3], A Schenck[1] and Y Ōnuki[2]

[1] Institute for Particle Physics of ETH Zurich, CH-5232 Villigen PSI, Switzerland
[2] Faculty of Science, Osaka University, Machikaneyama, Toyonaka, Osaka 560, Japan

Received 30 January 2004
Published 19 March 2004
Online at stacks.iop.org/JPhysCM/16/2421 (DOI: 10.1088/0953-8984/16/13/020)

Abstract

Monocrystalline $CeCu_2$ has been studied by muon-spin rotation and relaxation (μSR) spectroscopy, using transverse- and longitudinal-field techniques between 5 and 300 K for the paramagnetic state, and in zero field (ZF) for the ordered antiferromagnetic (AF) phase, $T_N \approx 3.6$ K. As in the isostructural orthorhombic compounds $GdCu_2$ and $PrCu_2$, in $CeCu_2$ the μ^+ is found at a 4e site. Bulk magnetic susceptibility and local susceptibility (extracted from the μ^+ Knight shift) are found to differ, most probably because of a change in crystalline electric field splitting of the Ce^{3+} ions next to the muon. The relaxation of the μ^+-spin polarization shows heavily anisotropic magnetic field fluctuations, explained by a dominant moment fluctuation amplitude along the crystallographic $\boldsymbol{b}$ axis. Below T_N, ZF measurements reveal a spontaneous μ^+ precession frequency. The corresponding static magnetic field pattern is consistent with the known AF structure; fields at the μ^+ and Ce moments are parallel to the $\pm\boldsymbol{c}$ axis. The temperature dependence of the μSR frequency is fitted by a two T-regime model, reflecting critical behaviour near T_N and magnon excitation at low T. The oriented Ce moment values extracted from neutron diffraction measurements are not consistent with the μSR results. Part of the discrepancy could possibly be explained by a change of the contact-hyperfine coupling parameter A_0 at low temperature.

(Some figures in this article are in colour only in the electronic version)

1. Introduction

Muon-spin rotation or relaxation (μSR) spectroscopy often discloses features of the magnetic order not observable or overlooked by other techniques. For instance, in $PrCu_2$ the modulated antiferromagnetic (AF) structure known to exist below $T_N \approx 60$ mK appears for μSR to persist on a short-range scale up to the astonishing temperature of 1000 T_N [1, 2]. In $GdCu_2$, the basic

[3] Author to whom any correspondence should be addressed.

AF order derived from neutron scattering measurements is confirmed by μSR spectroscopy [3], but the data allow a refinement of the structure as regards canting of the Gd moments and reveal unexpected temperature dependences. In $NdCu_2$, a μSR measurement indicates that a complete squaring up of the proposed AF-spin configuration is only effective below 1.2 K [4].

In continuation of the systematic μSR study of RCu_2 compounds (R = rare earth) [5], we present here results for $CeCu_2$ single crystals. Like most of the RCu_2 compounds they crystallize in the body-centred-orthorhombic $CeCu_2$-type structure (space group $Imma$, Ce at 4e and Cu at 8h sites). We have implanted positive muons in the samples and performed zero-, longitudinal-, and transverse-field (ZF, LF, TF) μSR measurements.

$CeCu_2$ is a Kondo lattice compound with AF order below $T_N \approx 3.6$ K and a Kondo temperature of about 6 K. The proposed magnetic structure is derived from neutron diffraction experiments [6, 7]. The magnetic moments of the two Ce ions in the chemical unit cell are antiparallel, aligned along the crystallographic c axis. $CeCu_2$ is the only compound of the isostructural RCu_2 series with its ordered moments in the $\pm\boldsymbol{c}$ direction. High-field magnetization measurements reveal a field-induced metamagnetic transition [8, 9], which is discussed in terms of the quadrupolar interaction and the crystalline electric field (CEF). For the Ce^{3+} ions in orthorhombic symmetry it is expected that the multiplet of the $J = 5/2$ Hund's rule ground state is split into three doublets due to CEF effects. Inelastic neutron scattering experiments have found excited levels at 9 meV (105 K) and 23 meV (268 K) above the ground state [10], and shown an unusual coupling between a crystal field transition and phonons [11].

2. Experimental details

The μSR measurements were performed at the Swiss Muon Source of the Paul Scherrer Institut (PSI), using the general purpose spectrometer GPS and the low temperature instrument LTF. Both spectrometers are supplied with surface μ^+ with essentially 100% spin polarization and 4 MeV kinetic energy.

The LTF allows us to select temperatures between ∼20 mK and a few kelvins; the GPS temperatures between 1.8 K and room temperature. In this latter spectrometer external fields $\boldsymbol{H}_{\rm ext}$ up to 6 kOe can be applied parallel to the incoming μ^+. In the LTF only zero-field measurements were performed.

The GPS allows us to monitor the decay positrons from the implanted μ^+ in five positron detectors placed in forward (F), backward (B), up (U), down (D), and right (R) directions with respect to the μ^+ beam momentum. In the LTF we used only the forward and backward placed positron detectors. The beam line is equipped with a spin rotator, therefore the polarization $\boldsymbol{P}_\mu(0)$ of the incoming μ^+ (spin pointing backwards) can be rotated up to ∼50°, from nearly parallel to the horizontal beam axis towards the vertical (up) direction. This feature (only used in the GPS) allows us, with an external field along the beam momentum, to perform TF measurements (looking at the U, D, and R detectors) in parallel with LF measurement (looking at the F and B detectors). A comprehensive description of the spectrometer and muon-beam characteristics can be found in [12].

The $CeCu_2$ single crystals were prepared at Osaka University; details are reported in [13]. A first sample, slightly wedge shaped, had a thickness of 2.3 mm (in the direction of the crystallographic c axis), a length of 5.7 mm (parallel to the a axis), and a base of 3.1 mm. A second sample, composed of two pieces, formed an elliptic plate with a long axis of ∼13 mm (the crystallographic a axis), a short axis of ∼10 mm, and a thickness of ∼0.8 mm (in direction of the crystallographic c axis). The first sample, used in the GPS instrument, could be rotated around its a axis oriented perpendicular to the beam or the applied field. Hence the initial polarization $\boldsymbol{P}_\mu(0)$ or $\boldsymbol{H}_{\rm ext}$ could be turned in the $\boldsymbol{bc}$ plane. To minimize the μSR signal not

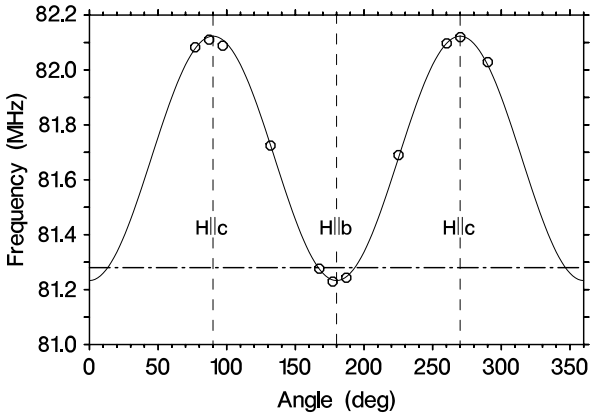

Figure 1. Crystal orientation dependence of the TF μSR frequency in $CeCu_2$ at 10 K. The crystal is rotated around its $\boldsymbol{a}$ axis with $\boldsymbol{H}_{\rm ext}$ in the $\boldsymbol{bc}$ plane. Solid curve: $\cos^2(\Theta)$ fit to the data points. Dot–dashed line: frequency corresponding to the external applied field, $H_{\rm ext} = 6$ kOe.

stemming from the $CeCu_2$ crystal, the sample was supported at the end of the sample holder solely by Mylar tape. The second sample was also hold with Mylar tape in the GPS, but in the LTF, where only this sample was used, it was glued on the silver cold finger and mounted with the fixed orientation $\boldsymbol{P}_\mu(0) \parallel \boldsymbol{c}$.

In a μSR experiment the evolution of the μ^+ polarization $\boldsymbol{P}_\mu(t)$ is monitored via the time-dependent decay asymmetry of the implanted μ^+ by observing the positrons from the μ^+ decay in a certain direction $\boldsymbol{r}$ as a function of elapsed μ^+ lifetime. The positron rate can then be written as [14]

$$\frac{{\rm d}N_{\rm e^+}(t)}{{\rm d}t} = \frac{1}{4\pi\tau_\mu} N_0 {\rm e}^{-t/\tau_\mu}[1 - A\boldsymbol{P}_\mu(t)\cdot\boldsymbol{r}]\,{\rm d}\Omega_r, \tag{1}$$

where A is the effective decay asymmetry (0.2−0.3), τ_μ the mean muon lifetime (2.2 μs), $|\boldsymbol{r}| = 1$ and ${\rm d}\Omega_r$ a solid angle element in the direction of $\boldsymbol{r}$. The product $AP_\mu(t) \equiv A\boldsymbol{P}_\mu(t)\cdot\boldsymbol{r}$ is often called asymmetry or signal amplitude. A μ^+ experiencing a local magnetic field $\boldsymbol{B}$ effectuates a Larmor precession around $\boldsymbol{B}$ with the frequency

$$\omega \equiv 2\pi\nu = \gamma_\mu|\boldsymbol{B}|. \tag{2}$$

γ_μ, the μ^+ gyromagnetic ratio, amounts to $\gamma_\mu = 2\pi \times 13.554$ MHz kG^{-1}.

3. TF and LF measurements

Transverse-field measurements were primarily performed in $CeCu_2$ to determine the μ^+ site from the μ^+ Knight shift by the standard procedure [15]. The muon precession frequency was measured in an applied field $\boldsymbol{H}_{\rm ext}$, $H_{\rm ext} = 6$ kOe, for various crystal orientations in the field, and as a function of temperature with 5 K $\leqslant T \leqslant$ 300 K.

In the paramagnetic state of $CeCu_2$ the data reveal a single-component signal with an anisotropic frequency shift. As an example, figure 1 shows the frequency as a function of the angle Θ between the applied field and the crystallographic b axis, with $\boldsymbol{H}_{\rm ext}$ staying in the $\boldsymbol{bc}$ plane. The temperature dependence of the μ^+ frequency for $\boldsymbol{H}_{\rm ext}$ either parallel to the crystallographic c axis ($\boldsymbol{H} \parallel \boldsymbol{c}$) or parallel to the b axis ($\boldsymbol{H} \parallel \boldsymbol{b}$) can be seen in figure 2. A notable positive frequency shift is observed for $\boldsymbol{H} \parallel \boldsymbol{c}$, whereas the shift is smaller and negative for $\boldsymbol{H} \parallel \boldsymbol{b}$.

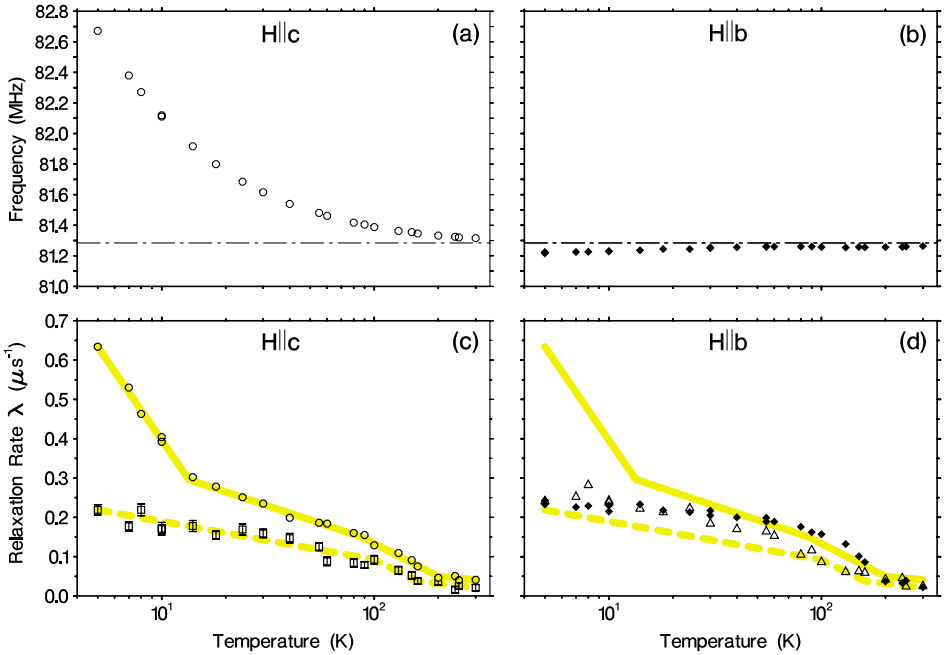

Figure 2. Frames (a) and (b): temperature dependence of TF μSR frequency for two orientations of the $CeCu_2$ crystal. Dot–dashed line: frequency corresponding to the external applied field. (c): TF (circles) and LF (squares) relaxation rates for $\boldsymbol{H} \parallel \boldsymbol{c}$. (d): TF (diamonds) and LF (triangles) relaxation rates for $\boldsymbol{H} \parallel \boldsymbol{b}$. The solid and dashed grey lines for $\boldsymbol{H} \parallel \boldsymbol{c}$ (c) are guides to the eye and have been included in (d) for comparison.

3.1. μ^+ Knight shift

To obtain the Knight shifts from the shifts of the precession frequencies one has to correct for demagnetization and Lorentz fields, which necessitates knowledge of the bulk magnetic susceptibility of the sample. The temperature dependence of the inverse bulk susceptibility χ^{-1} is shown in figure 3 [16]. A large anisotropy is visible; for $\boldsymbol{H} \parallel \boldsymbol{a}$ and $\boldsymbol{H} \parallel \boldsymbol{c}$ the susceptibility follows a Curie–Weiss (CW) relation above 200 K (straight solid lines in figure 3), written here as

$$\chi_i = \frac{C}{T - T_{\mathrm{C},i}}, \qquad i = a, c. \tag{3}$$

C is the Curie–Weiss constant, with theoretical value $C = \frac{NJ(J+1)}{3k_\mathrm{B}} g_J^2 \mu_\mathrm{B}^2$, which amounts to 0.0231 K (or 0.807 K emu mol^{-1}) for Ce ions. If left as a free parameter, the values yielded by fits to χ_a and χ_c differ only slightly from the theoretical figure, and the variation has no implication for the following. The related parameters can be found in table 1. For $\boldsymbol{H} \parallel \boldsymbol{b}$ the susceptibility does not show CW behaviour below 300 K.

For the demagnetization correction, the demagnetization factors of the sample are estimated using tabulated values [17]. The resulting temperature dependence of the Knight shift for two crystal orientations in the field are shown in figure 4. For $\boldsymbol{H} \parallel \boldsymbol{c}$ a CW law fits the data very well above 70 K. For $\boldsymbol{H} \parallel \boldsymbol{b}$ the temperature dependence is peculiar, reminiscent of the corresponding bulk susceptibility component behaviour (though with opposite sign), and it cannot be simply described by a Curie–Weiss relation.

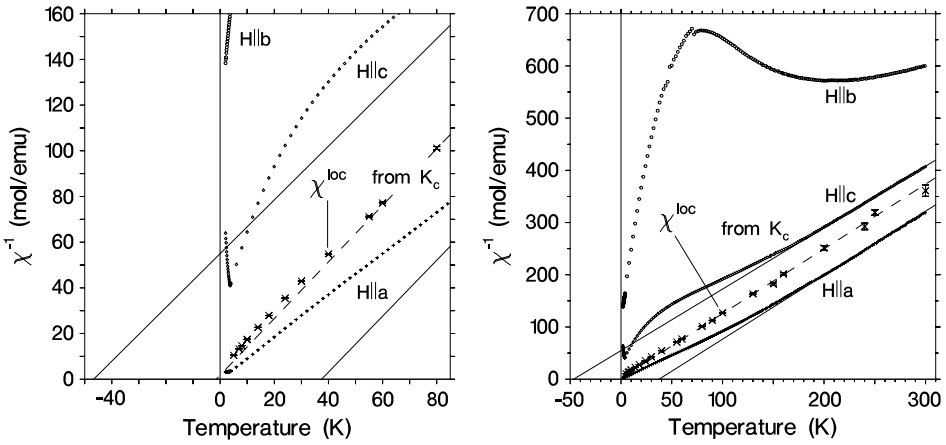

Figure 3. Temperature dependence of the inverse magnetic susceptibility in $CeCu_2$, from [16]. Right-hand panel: full T range; left-hand panel: expanded low-T range. The CW behaviour for $\boldsymbol{H} \parallel \boldsymbol{a}$ and $\boldsymbol{H} \parallel \boldsymbol{c}$ above 200 K is indicated by the solid lines. Symbol $\times$: inverse of the *local* susceptibility for $\boldsymbol{H} \parallel \boldsymbol{c}$, $\chi_c^{\rm loc}$, deduced from the $\mu^+ K_c$ measurements; dashed line: CW approximation of $\chi_c^{\rm loc}$ above 70 K (see section 3.2).

Table 1. Bulk susceptibility and μ^+ Knight-shift components for $CeCu_2$ fitted by a Curie–Weiss relation, equations (3) and (9), respectively, with deduced parameters. (K_a has not been measured, and for χ_b ($T < 300$ K) a CW fit is not possible.)

χ_i, K_i	Fit range (K)	C_i^* (K)	C (K emu mol^{-1})	$A_i = C_i^*/C$ (mol emu^{-1})	$T_{{\rm C},i}$ (K)	$A_{0,i}^{\rm a}$ (mol emu^{-1})	K_i^0 ($\times 10^{-6}$)
χ_a	210–290	—	0.816(10)	—	+37.5(9)	—	—
χ_c	210–290	—	0.85(2)	—	−47(2)	—	—
$K_c^{\rm b}$	70–300	0.146(8)	0.807	0.181(9)	−1(3)	0.150(11)	−82(27)
$K_c^{\rm c}$	70–300	0.146(8)	0.85	0.172(9)	−1(3)	0.141(10)	−82(27)

[a] For K_c, μ^+ assumed at the 4e site with $z_\mu = 0.862$.
[b] With the theoretical value of C.
[c] Alternative result with C from the CW fit of χ_c; gives a marginal change for $A_{0,c}$.

3.2. Muon site

In general one assumes that the Knight shift consists of two contributions: a contact-hyperfine term and a dipolar field term. The dipolar field originates from the moments induced by the external field $\boldsymbol{H}_{\rm ext}$, and the contact term arises from the spin polarization of the conduction electrons at the μ^+ site. The spin polarization is dominantly caused via the RKKY mechanism by the moments induced in the 4f shell of Ce^{3+} and should scale with the magnetic susceptibility. As usual we may write [15]

$$K_a = (A_0 + A_{aa}^{\rm dip})\chi_a + K_a^0, \tag{4}$$

$$K_b = (A_0 + A_{bb}^{\rm dip})\chi_b + K_b^0, \tag{5}$$

$$K_c = (A_0 + A_{cc}^{\rm dip})\chi_c + K_c^0, \tag{6}$$

where A_0 is the contact-coupling constant assumed to be isotropic and temperature independent, and $A_{ii}^{\rm dip}$ are the diagonal elements of the dipolar coupling tensor $\overleftrightarrow{A}^{\rm dip}$ with

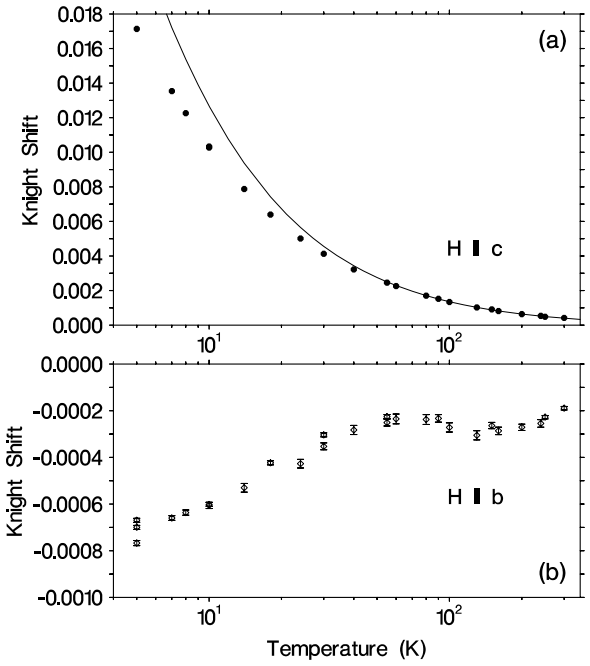

Figure 4. Temperature dependence of the μ^+ Knight shift in $CeCu_2$. (a): $\boldsymbol{H} \parallel \boldsymbol{c}$, a CW law fits the data for $T \geqslant 70$ K, solid curve; (b): $\boldsymbol{H} \parallel \boldsymbol{b}$.

$\sum A_{ii}^{\mathrm{dip}} = 0$. The χ_i are the components of a local susceptibility tensor $\overleftrightarrow{\chi}^{\mathrm{loc}}$ which characterizes the magnetic response of the Ce ions in the neighbourhood of the μ^+; they are basically responsible for the temperature dependences of the K_i components. The K_i^0 are small T-independent contributions, essentially reflecting the Pauli spin paramagnetism.

If a scaling of Knight shift with bulk susceptibility is observed, a possible path to find the μ^+ site is, for example, starting from the $K_b(T)$ and $K_c(T)$ measurements, to use the transformed equations (5), (6):

$$\Delta K_b/\Delta\chi_b = A_0 + A_{bb}^{\mathrm{dip}}, \tag{7}$$

$$\Delta K_c/\Delta\chi_c = A_0 + A_{cc}^{\mathrm{dip}}, \tag{8}$$

with the left-hand side values known from the experiment, assuming that the *local* susceptibility corresponds to the *bulk* susceptibility. A_0 and the difference of the dipolar tensor elements $A_{bb}^{\mathrm{dip}} - A_{cc}^{\mathrm{dip}}$ are then readily obtained. If the μ^+-site candidates are not too peculiar, the comparison of calculated and experimentally obtained $A_{bb}^{\mathrm{dip}} - A_{cc}^{\mathrm{dip}}$ normally leads to an unambiguous result.

In figure 5 we have plotted the measured μ^+ Knight shifts versus the related bulk susceptibilities (Clogston–Jaccarino plots). One expects a linear scaling between K_i and χ_i (equations (5), (6)), at least at high temperatures. A deviation from linear scaling points either to a local magnetic susceptibility at the μ^+ (possibly muon-induced) different from the bulk susceptibility (see, e.g., [18]) and/or to an unusual behaviour of the contact hyperfine constant [19]. Whereas figure 5 shows that for $\boldsymbol{H} \parallel \boldsymbol{b}$ it is possible to determine the slope $\Delta K_b/\Delta\chi_b$ at least for $T \geqslant 14$ K, it appears that for $\boldsymbol{H} \parallel \boldsymbol{c}$ the determination of $\Delta K_c/\Delta\chi_c$ is not feasible due to the non-linear K_c versus χ_c relation up to the high-T points.

There is, however, an alternative to this shortcoming. We have seen that above 70 K K_c shows a perfect Curie–Weiss temperature dependence, figure 4(a), which can be written

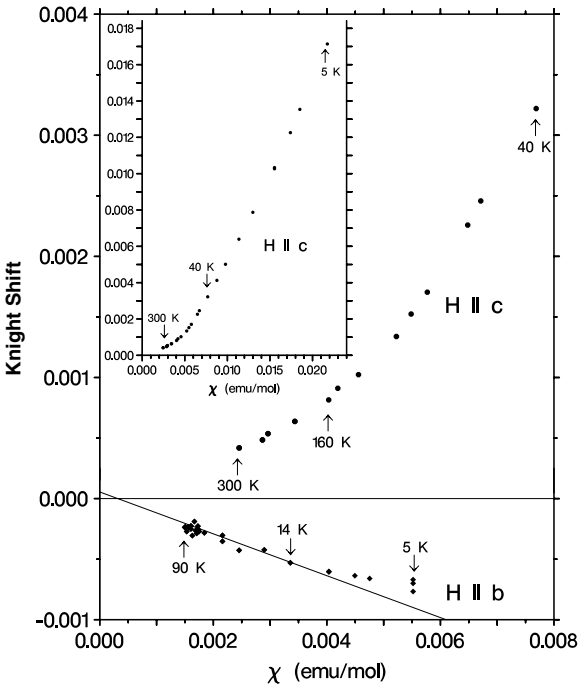

Figure 5. Muon Knight shift K_μ represented versus bulk magnetic susceptibility (Clogston–Jaccarino plot) for the two crystal orientations $\boldsymbol{H} \parallel \boldsymbol{c}$ ($K_c > 0$) and $\boldsymbol{H} \parallel \boldsymbol{b}$ ($K_b < 0$). For this latter orientation the linear scaling indicated by the solid straight lines is retained to determine the μ^+ site. For $\boldsymbol{H} \parallel \boldsymbol{c}$ (the full T range studied is shown in the inset) K_c does not scale linearly with the bulk χ_c.

$$K_c = \frac{C_c^*}{T - T_{\mathrm{C},c}} + K_c^0 \equiv \frac{A_c C}{T - T_{\mathrm{C},c}} + K_c^0, \tag{9}$$

where C_c^* is an 'effective' Curie–Weiss constant, $T_{\mathrm{C},c}$ a CW temperature, and K_c^0 a temperature independent contribution. Although the loss of K_c versus χ_c (bulk) scaling can be attributed to a μ^+ induced modification of the magnetic response of the nearest Ce neighbours, the ionic state of Ce, i.e. Ce^{3+}, cannot be changed. Hence the factor C can be identified with the theoretical Curie–Weiss constant, and A_c stands for $A_0 + A_{cc}^{\mathrm{dip}}$, i.e.,

$$C_c^*/C = A_0 + A_{cc}^{\mathrm{dip}} \tag{10}$$

is a relation which replaces now equation (8). The CW fit results for K_c are listed in table 1. The local susceptibility χ_c^{loc} deduced by this procedure from the Knight shift K_c is also shown, together with its CW approximation, in figure 3. As can be seen, even below 70 K χ_c^{loc} is rather close to the CW approximation. On the other hand the difference between bulk and local susceptibility is important; it should be mentioned that similar differences have been observed before, for example in $U_{14}Au_{51}$ [20] and in $PrCu_2$ [2].

Hence equations (7) and (10) lead to

$$A_{bb}^{\mathrm{dip}} - A_{cc}^{\mathrm{dip}} = \Delta K_b/\Delta\chi_b - C_c^*/C, \tag{11}$$

allowing comparison between calculation and measurement.

The orthorhombic $CeCu_2$-type structure is shown in figure 6. From all possible μ^+-site candidates, as in other RCu_2 compounds [1, 3], only the 4e site, at the generic position $(0, \frac{1}{4}, z_\mu)$, turns out to be adequate. The search of the muon site is now reduced to the determination of the z_μ co-ordinate value (table 2).

Assuming an undistorted $CeCu_2$ lattice, the tensor $A_{\kappa\lambda}^{\mathrm{dip}}$ can easily be calculated. In figure 7 the determined $\Delta K_b/\Delta\chi_b - C_c^*/C = -1.97(16)$ kG/μ_{B} (the important part of the error stems

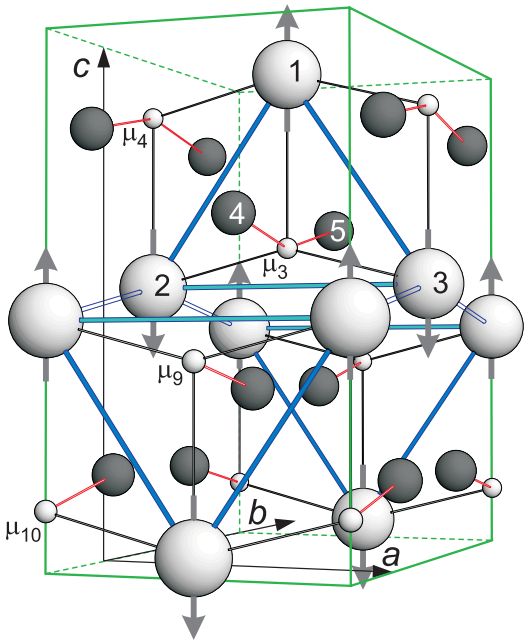

Figure 6. Unit cell of the orthorhombic $CeCu_2$ crystal containing 4 rare-earth ions at 4e sites (large light spheres) and 8 Cu ions at 8h sites (medium-size dark spheres), arranged in four double layers parallel to the *ab* basal plane. The determined μ^+ sites, 4e, are also indicated (small spheres). The magnetic structure of $CeCu_2$ below T_N [6, 7] is shown by the moments of the Ce ions.

Table 2. Lattice, μ^+-position, and various other parameters in three RCu_2 compounds. For the atom labels see figure 6. A lattice relaxation around the μ^+ is not considered.

Parameter or co-ordinate	$CeCu_2$	$PrCu_2$	$GdCu_2$
a (Å)	4.42	4.40	4.305
b (Å)	7.04	7.024	6.848
c (Å)	7.45	7.435	7.306
z_R of ion R at co-ord. $(0, \frac{1}{4}, z_R)$	0.538	0.538	0.538
z_μ of μ^+ at co-ord. $(0, \frac{1}{4}, z_\mu)$	0.862(6)	0.8594(4)	0.887(4)
Dist. R2–R3 ('base') = a (Å)	4.42	4.40	4.30
Dist. R1–R2 or R3 (Å)	3.86	3.85	3.78
Dist. Cu4–Cu5 (Å)	4.24	4.23	4.12
Dist. μ_3^+–R1 ('apical') (Å)	2.42	2.39	2.55
Dist. μ_3^+–R2 or R3 ('basal') (Å)	2.33	2.33	2.22
Dist. μ_3^+–Cu4 or Cu5 (Å)	2.13	2.12	2.10
A_0 (kG/μ_B)	0.839(61)	0.709(3)	—

from the determination of $\Delta K_b/\Delta\chi_b$) is compared to $A_{bb}^{dip} - A_{cc}^{dip}$ calculated for the 4e site as a function of z_μ. The result $z_\mu = 0.862 \pm 0.006$ is obtained, corresponding to a μ^+ position not far from being equidistant to the three nearest Ce ions of the rare-earth triangle in the *ac* plane. This result is listed in table 2, which also contains other parameters concerning the $CeCu_2$, $PrCu_2$ [2], and $GdCu_2$ [3] lattices. For $CeCu_2$, using equation (7), one deduces in turns $A_0 = 0.839(61)$ kG μ_B^{-1} or $0.150(11)$ mol emu^{-1} for the contact-coupling constant.

3.3. Spin–lattice relaxation

Figure 2 also shows the relaxation rates of the TF signals and those of the LF components measured at the same time. Oscillating TF and non-oscillating LF data are both well fitted by

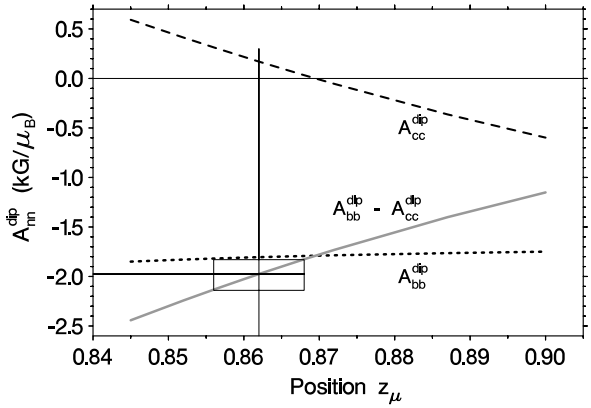

Figure 7. Calculated dipolar-coupling tensor components $A_{bb}^{\rm dip}$ and $A_{cc}^{\rm dip}$ as functions of the muon co-ordinate z_μ, dotted and dashed lines, for the body-centred-orthorhombic structure of $CeCu_2$ (space group $Imma$), μ^+ at the generic site $(0, \frac{1}{4}, z_\mu)$. The $A_{bb}^{\rm dip} - A_{cc}^{\rm dip}$ value deduced from TF-μSR measurements and the inferred z_μ with corresponding error intervals are indicated by the rectangular box on the grey $A_{bb}^{\rm dip} - A_{cc}^{\rm dip}$ line.

exponential relaxation functions, with rates $\lambda_i^{\rm TF}$ and $\lambda_i^{\rm LF}$, respectively ($i = c, b$). The fact that the TF relaxation is Lorentzian rather than Gaussian is a strong indication that the accountable process is of dynamical origin. Also, in LF $\lambda_i^{\rm LF}$ is not much different from $\lambda_i^{\rm TF}$, except perhaps below 14 K. It is, however, not an absolute proof of the absence of static (or quasi-static) fields responsible for the TF relaxation, which is known to result from the dephasing (increasing with time) of the precessing muon-spin ensemble. Indeed, the dipolar fields resulting from a diluted static spin system around the μ^+ lead precisely to Lorentzian relaxation functions [21]. We will come back to this possibility in the discussion of the behaviour of $\lambda_c^{\rm TF}$ below $\sim$14 K. For the time being, we consider the relaxations as resulting from dynamical effects (with the mentioned reservation in TF for $T \lesssim 14$ K). In this case TF and LF relaxation rates can be described by the Redfield theory [22]. For the crystal orientation with $\boldsymbol{H} \parallel \boldsymbol{c}$ one gets

$$\lambda_c^{\rm LF} = \frac{1}{T_1} = \gamma_\mu^2(\overline{B_a^2} + \overline{B_b^2})\frac{\tau_0}{1+\omega^2\tau_0^2}, \tag{12}$$

$$\lambda_c^{\rm TF} = \frac{1}{T_2} = \gamma_\mu^2\overline{B_c^2}\tau_0 + \frac{1}{2T_1} = \gamma_\mu^2\left[\overline{B_c^2}\tau_0 + \frac{1}{2}(\overline{B_a^2} + \overline{B_b^2})\frac{\tau_0}{1+\omega^2\tau_0^2}\right], \tag{13}$$

where $\overline{B_i^2}$ is the averaged square amplitude of the *fluctuating* magnetic field component in direction i at the μ^+, τ_0 the correlation time of the fluctuating fields, and ω the muon Larmor frequency in the total *static* field at the μ^+. For $\boldsymbol{H} \parallel \boldsymbol{b}$ one has, correspondingly,

$$\lambda_b^{\rm LF} = \gamma_\mu^2(\overline{B_a^2} + \overline{B_c^2})\frac{\tau_0}{1+\omega^2\tau_0^2}, \tag{14}$$

$$\lambda_b^{\rm TF} = \gamma_\mu^2\left[\overline{B_b^2}\tau_0 + \frac{1}{2}(\overline{B_a^2} + \overline{B_c^2})\frac{\tau_0}{1+\omega^2\tau_0^2}\right]. \tag{15}$$

As one increases τ_0 (slows the motion), the validity of the Redfield equations (12)–(15) ceases when $T_2 \cong \tau_0$, i.e., when $\tau_0 \cong 1/\left(\gamma_\mu\sqrt{\overline{B_c^2}}\right)$ or $\tau_0 \cong 1/\left(\gamma_\mu\sqrt{\overline{B_b^2}}\right)$, respectively. Within the domain of validity, as a function of τ_0, the theoretical $1/T_1$ goes through a maximum for $\tau_0 \cong 1/\omega$. In our data, figures 2(c), (d), taken in a field of 6 kOe, i.e. with

$\omega = 5.11 \times 10^8$ rad s^{-1}, no maximum of λ_c^{LF} or λ_b^{LF} is seen. Also, in a measurement series with LF = 100 Oe the relaxation rates λ_c^{LF} and λ_b^{LF} obtained with LF = 6 kOe are well reproduced. (On the other hand ZF measurements performed between 8 and 80 K yield $\lambda_b^{\mathrm{ZF}} \approx 1.5\,\lambda_b^{\mathrm{LF}}$ and $\lambda_c^{\mathrm{ZF}} \approx 1.9\lambda_c^{\mathrm{LF}}$.) Hence, for the studied temperature range with $T \geqslant 5$ K, no field effect is visible, implying that in the Redfield formulae one always has $\omega^2\tau_0^2 \ll 1$—so τ_0 stays clearly below 2 ns. Therefore, equations (12)–(15) can be replaced by

$$\lambda_c^{\mathrm{LF}} = \gamma_\mu^2(\overline{B_a^2} + \overline{B_b^2})\tau_0 = F_c^{\mathrm{LF}}\tau_0, \tag{16}$$

$$\lambda_c^{\mathrm{TF}} = \gamma_\mu^2[\overline{B_c^2} + \tfrac{1}{2}(\overline{B_a^2} + \overline{B_b^2})]\tau_0 = F_c^{\mathrm{TF}}\tau_0, \tag{17}$$

$$\lambda_b^{\mathrm{LF}} = \gamma_\mu^2(\overline{B_a^2} + \overline{B_c^2})\tau_0 = F_b^{\mathrm{LF}}\tau_0, \tag{18}$$

$$\lambda_b^{\mathrm{TF}} = \gamma_\mu^2[\overline{B_b^2} + \tfrac{1}{2}(\overline{B_a^2} + \overline{B_c^2})]\tau_0 = F_b^{\mathrm{TF}}\tau_0, \tag{19}$$

defining at the same time four 'fluctuation factors' F_i^α, $\alpha = \mathrm{LF}, \mathrm{TF}$.

With $\boldsymbol{H} \parallel \boldsymbol{c}$, the ratio of the measured rates $\lambda_c^{\mathrm{TF}}(T)/\lambda_c^{\mathrm{LF}}(T)$, i.e. $F_c^{\mathrm{TF}}/F_c^{\mathrm{LF}}$, starts around 3 at 5 K, drops smoothly to 1.7 at 20 K, then to 1.5 at 50 K, and is more or less stable around 1.8 for the higher temperatures. With $\boldsymbol{H} \parallel \boldsymbol{b}$, the ratio of the measured rates $\lambda_b^{\mathrm{TF}}(T)/\lambda_b^{\mathrm{LF}}(T)$ is close to 1.1 for all temperatures (except between 80 and 150 K, where it fluctuates around 1.4). Finally, the ratio $\lambda_b^{\mathrm{LF}}(T)/\lambda_c^{\mathrm{LF}}(T)$ is ∼1.3 for all temperatures. This can all be very well approximated by T-independent ratios $F_c^{\mathrm{TF}}/F_c^{\mathrm{LF}}$, $F_b^{\mathrm{TF}}/F_b^{\mathrm{LF}}$, and $F_b^{\mathrm{LF}}/F_c^{\mathrm{LF}}$, assuming

$$\overline{B_b^2} = 5\overline{B_a^2}, \tag{20}$$

$$\overline{B_c^2} = 7\overline{B_a^2}. \tag{21}$$

Below 14 K the peculiar behaviour of λ_c^{TF}, which increases monotonously with decreasing T and reaches at 5 K a value of almost twice the otherwise consistent Redfield value, has to be explained by a broadening of the distribution of the *static* field component B_c for the muon ensemble.

On the higher temperature side, looking at λ_i^{TF} and λ_i^{LF} in figure 8, which shows $\log(1/\lambda)$ versus $1/T$ for $T \geqslant 14$ K, one observes a change of regime at ∼100 K, possibly indicating the occurrence of muon diffusion above that temperature. As is often the case for motions across a barrier [22], one can assume that for $T > 100$ K the correlation time is τ_1, the inverse of a hopping rate, given by the Arrhenius relation

$$\tau_1 = \tau_{\infty,1} \exp(E_{\mathrm{a},1}/k_{\mathrm{B}}T), \tag{22}$$

where $E_{\mathrm{a},1}$ is the activation energy and $\tau_{\infty,1}$ the value of τ_1 for infinite temperature. In addition, one can also assume that in the region 100 K $> T >$ 14 K another Arrhenius relation with τ_2 defined by $E_{\mathrm{a},2}$ and $\tau_{\infty,2}$ is essentially governing the correlation time. Hence, the combined correlation rate $1/\tau_0$ is the sum $1/\tau_0 = 1/\tau_1 + 1/\tau_2$, which, introduced in equations (16)–(19), leads for the inverse of the measured relaxation rates λ_i^α to the expression

$$1/\lambda_i^\alpha \equiv \Gamma_{R,i}^\alpha(T) = (1/F_i^\alpha)(1/\tau_1 + 1/\tau_2). \tag{23}$$

Assuming for the temperature dependences $\Gamma_{R,i}^\alpha(T)$ the relations between the squared fluctuation amplitudes indicated by equations (20), (21), one can quite reasonably fit the data, as shown by the solid curves in figure 8. The fit parameters are listed in table 3.

It is not possible to ascribe the anisotropy of the fluctuating fields (equations (20), (21)) simply to the random isotropic fluctuation of the magnetic moments connected to the Ce atoms of the lattice. Indeed, for such a case the proper evaluation of the second moment Δ^2 of the field distribution at the μ^+ site gives for the corresponding components the relations $\Delta_b^2 = 1.55\Delta_a^2$ and $\Delta_c^2 = 1.24\Delta_a^2$, with $\Delta_a^2 \approx 2.4 \times 10^6$ G^2, quite different from the anisotropy implied by equations (20) and (21).

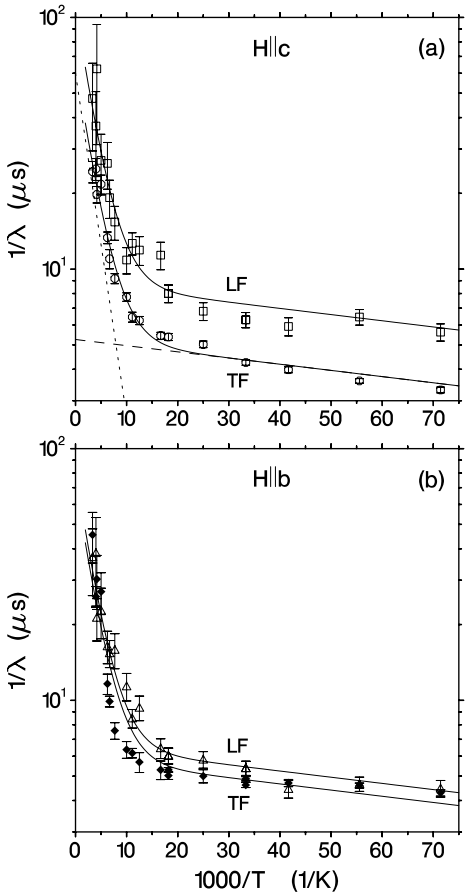

Figure 8. Arrhenius plots of $1/\lambda_c^{\mathrm{TF}}$ (circles), $1/\lambda_c^{\mathrm{LF}}$ (squares) in the upper panel, of $1/\lambda_b^{\mathrm{TF}}$ (diamonds) and $1/\lambda_b^{\mathrm{LF}}$ (triangles) in the lower panel. The solid curves correspond to fits with equation (23) for $T > 14$ K; see the text. For $1/\lambda_c^{\mathrm{TF}}$, for example, the contributions of the two involved Arrhenius components are indicated by dotted and dashed lines.

Table 3. Parameters for the fit of the $1/\lambda_i^{\alpha}$ data with equation (23) for $T > 14$ K (figure 8).

α	i	$E_{\mathrm{a},1}$ (meV)	$(F_i^{\alpha} \times \tau_{\infty,1})^{-1}$ ($\times 10^{-6}$ s)	$E_{\mathrm{a},2}$ (meV)	$(F_i^{\alpha} \times \tau_{\infty,2})^{-1}$ ($\times 10^{-6}$ s)
LF	$\boldsymbol{H} \parallel \boldsymbol{c}$	27.0(2.3)	100	0.49(7)	8.8
TF	$\boldsymbol{H} \parallel \boldsymbol{c}$	27.0(2.3)	60	0.49(7)	5.3
LF	$\boldsymbol{H} \parallel \boldsymbol{b}$	27.0(2.3)	75	0.49(7)	6.6
TF	$\boldsymbol{H} \parallel \boldsymbol{b}$	27.0(2.3)	67	0.49(7)	5.8

Likewise, the anisotropy cannot stem from the nuclear magnetic moment of the Cu ion (the only atom of $CeCu_2$ with a nuclear moment) 'fluctuating', for example, because of the random hopping of the diffusing μ^+: the related second-moment components are $\Delta_{N,a}^2 = 1.78\,\Delta_{N,b}^2$, $\Delta_{N,c}^2 = 1.65\,\Delta_{N,b}^2$, with $\Delta_{N,b}^2 \approx 6.4\,\mathrm{G}^2$. Besides the inadequate anisotropy, the small second-moment values would imply far too long hopping times, rendering the Redfield formulae inapplicable.

In conclusion, a *fully random* fluctuation of neither the electronic Ce moments nor the nuclear Cu moments can produce the observed field fluctuations. However, a random fluctuation of the Ce moments restricted essentially to the crystallographic ***bc*** plane could

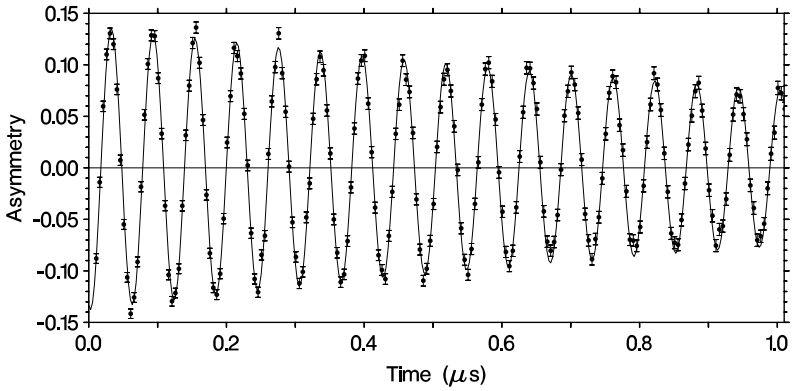

Figure 9. ZF μSR asymmetry spectrum for $CeCu_2$ with $\boldsymbol{b} \parallel \boldsymbol{P}_\mu(0)$ measured at 1.1 K (first μs, forward detector, LTF spectrometer). Solid line: fitted function $-A_F \exp(-\lambda t)\cos(2\pi\nu t + \phi)$.

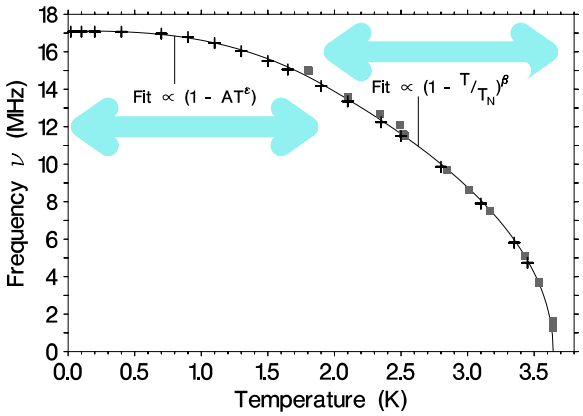

Figure 10. Temperature dependence of the ZF spontaneous μ^+ precession frequency observed for $\boldsymbol{b} \parallel \boldsymbol{P}_\mu(0)$ in $CeCu_2$ with the LTF (crosses) and the GPS (squares) spectrometer. An empirical two T-regime dependence (solid curve) has been fitted to the data.

be considered. Indeed, a crude calculation shows that observed field fluctuations mainly noticeable in the $\boldsymbol{b}$ and $\boldsymbol{c}$ directions, as indicated by equations (20) and (21), can be caused by the Ce moments fluctuating in the $\boldsymbol{bc}$ plane if the dominant moment fluctuation amplitude is along the $\boldsymbol{b}$ axis, perpendicular to the plane determined by the Ce triangles.

4. ZF measurements

Zero-field μSR measurements have been performed from 0.02 to 4.1 K. (As mentioned in section 3.3 ZF measurements have also been performed in the paramagnetic state, for 8 K $\leqslant T \leqslant$ 80 K.) A spontaneous precession frequency ν is observed below T_N for the incident-muon polarization $\boldsymbol{P}_\mu(0)$ oriented parallel to the crystallographic b axis ($\boldsymbol{P}_\mu(0) \parallel \boldsymbol{b}$); see, for example, figure 9. The temperature dependence of ν is shown in figure 10. No spontaneous oscillation is observed for $\boldsymbol{P}_\mu(0) \parallel \boldsymbol{c}$, i.e., the local fields are parallel to the c axis. The observed frequency is nearly constant below 0.4 K, then decreases with increasing T and

Table 4. Relevant parameters of a two T-regime fit to the temperature dependent spontaneous μSR frequency observed with $\boldsymbol{b} \parallel \boldsymbol{P}_\mu(0)$ in $CeCu_2$.

Parameter	Value	T-regime
ν_0 (MHz)	17.11(5)	$0 < T \leqslant T_r$
ϵ	2.6(1)	$0 < T \leqslant T_r$
T_r (K)	1.9(3)	Both
ν_h (MHz)	20.51(7)	$T_r \leqslant T < T_N$
β	0.50(1)	$T_r \leqslant T < T_N$

drops quickly to zero at T_N. The exponential damping rate of the signal is about 1 μs^{-1} at low T, decreases to a flat minimum of 0.5 μs^{-1} at 1.6 K, and then increases, probably because of the frequency broadening resulting from a small variation of sample temperature in this domain of stronger frequency change with temperature. The spontaneous frequency is very well fitted with an empirical two T-regime dependence: Above a *regime-transition temperature* T_r ($\sim T_N/2$), in the domain of critical behaviour, we can fit the data with a function of the form

$$\nu(T) = \nu_h[1 - (T/T_N)]^\beta, \tag{24}$$

whereas for $0 < T \leqslant T_r$, in the domain of magnon effects, we describe the frequency with

$$\nu(T) = \nu_0(1 - AT^\epsilon). \tag{25}$$

We request continuity of $\nu(T)$ and its first derivative at T_r. Such a field behaviour was previously encountered in $GdCu_2$ [3]. The result of the fit is reported in table 4; the parameters are rather insensitive to a variation of T_r for $0.4T_N < T_r < 0.6T_N$.

The critical behaviour parameter β (equation (24)) yielded by the fit has a value of 0.50(1), corresponding exactly to a simple mean-field calculation [23]. It is, however, only marginally compatible with the value $\beta = 0.34(9)$ obtained rather indirectly for the $CeCu_2$-sublattice magnetization by zero-field neutron polarimetry [7]. In the temperature regime of the magnon effects (equation (25)) the determined exponent $\epsilon = 2.6(1)$ is larger than 2.0 obtained from a calculation for a cubic 3D antiferromagnet [24]. To our knowledge, the temperature dependence of the sublattice magnetization due to magnon excitations in an orthorhombic structure has not been calculated yet.

Taking the AF structure proposed by Trump *et al* [6] and Nunez *et al* [7], with magnetic moments $\boldsymbol{\mu}$ of the Ce atoms parallel and antiparallel to the orthorhombic c axis (see the moments in figure 6), one can calculate for our muon location a dipolar magnetic field sum $\boldsymbol{B}_{dip}$. Retaining now the value $|\boldsymbol{\mu}| = 0.33(2)\ \mu_B$/Ce atom at 2.5 K indicated in [7] (at this temperature the sublattice magnetization has not attained its saturation value), we find dipolar fields $\boldsymbol{B}_{dip}$ parallel or antiparallel to the c axis, corresponding to a unique precession frequency of 9.17 MHz. We have to consider in addition the presence of a contact-hyperfine field $\boldsymbol{B}_0$ induced by the moments $\boldsymbol{\mu}$ at the three Ce neighbours next to the μ^+ at the position $\boldsymbol{R}_\mu$:

$$\boldsymbol{B}_0(\boldsymbol{R}_\mu) = A_0 \sum_{i=1}^{3} \boldsymbol{\mu}(\boldsymbol{R}_\mu + \boldsymbol{r}_i), \tag{26}$$

where $\boldsymbol{r}_i = \boldsymbol{R}_i - \boldsymbol{R}_\mu$, with $\boldsymbol{R}_i$ denoting the position of the Ce ions. Taking $A_0 = 0.839\ \mathrm{kG}/\mu_B$ obtained above, we calculate $|\boldsymbol{B}_0(\boldsymbol{R}_\mu)| = 277$ G, i.e. 3.75 MHz, with $\boldsymbol{B}_0$ *antiparallel* to the dipolar field. Therefore, the calculated total field conserves the same orientation as $\boldsymbol{B}_{dip}$, but is smaller, corresponding to a μSR frequency of 5.42 MHz. This value is compared to the obtained μ^+ frequency $\nu(T)$ in figure 11. At 2.5 K we observe the spontaneous frequency at 11.6 MHz. Hence, the quoted Ce moment value [7] appears too small. This discrepancy

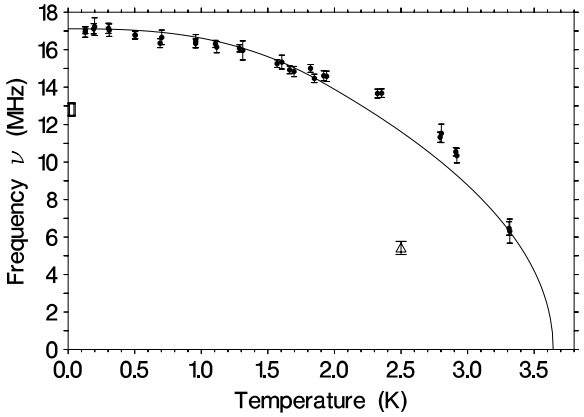

Figure 11. Temperature dependence of the ZF spontaneous μ^+ precession frequency observed for $b \parallel P_\mu(0)$ in $CeCu_2$ (solid fit curve, from figure 10) compared to the normalized square root of the intensity of the (110) and (130) n-diffraction reflections (circles) [25] and the points at 2.5 K (triangle) [7] and at 0 K (rectangle) [25] inferred from n-diffraction experiments.

cannot be reduced substantially by modifying the μ^+ positions along the c axis: a (reasonable) variation of z_μ by 7% changes the calculated field by less than 4%.

To explain the saturation value of the local field observed below 0.2 K, i.e., 1263 G corresponding to 17.11 MHz, one needs, assuming the mentioned AF structure, a moment $\mu_s = 1.04\ \mu_B$/Ce atom. In this calculation no crystal-lattice relaxation around the μ^+ is considered. (One estimates that a radial displacement of the nearest Ce neighbours away from the μ^+ by $\Delta r/r = +5\%$, with the rest of the lattice unchanged, leads to an attenuation of the field at the μ^+ site by $\Delta B/B \approx -25\%$. For such a crystal relaxation a saturation moment of 1.4 μ_B/Ce atom would be needed to account for the 17.11 MHz seen by the muon.)

The T dependence of the spontaneous μSR signal can be compared to the results of a neutron diffraction experiment [25]. In figure 11 we show the μ^+ frequency versus T together with the square root of the intensities corresponding to the (110) and (130) n-diffraction reflections, normalized to the muon frequency at low temperature. Except for a few points between 2.2 and 3.0 K, the agreement is very good. We do not, at this point, elaborate further on similarities or differences for the μ^+ and n results since these neutron data are poorly documented. From the same neutron measurements a saturation magnetic moment of 0.78(2) μ_B/Ce is inferred [25]. This would result in a μSR frequency of 12.8 MHz, also displayed at $T = 0$ K in figure 11, clearly inconsistent with the measured value.

5. Variable contact-hyperfine coupling, muon-induced effects

The discrepancy between the saturation moments resulting from neutron and muon data may indicate that either the value of 0.78(2) μ_B/Ce is incorrect, or the calculation of the expected μ^+ spontaneous precession frequency, using the saturation value from the neutron work, is wrong. However, once the μ^+ site is known the dipolar fields from the ordered moments can be calculated exactly.

One possibility for a modified calculation result is that the contact-coupling constant taken over from the high temperature Knight-shift measurements has become different below T_N. Indeed, reducing A_0 from 0.839 kG/μ_B to ~0.43 kG/μ_B, one can reproduce the measured

frequency exactly. Such a change of A_0 in the ordered phase has recently been observed in $PrCu_2$ [2] and CeAg [26] and has been attributed to quadrupolar effects leading to an orientation dependent exchange integral in the RKKY interaction. Such an effect could also cause in part deviation of the local susceptibility from the bulk susceptibility. Notice that quadrupolar interactions and CEF have also been used in $CeCu_2$ (as well as in RCu_2 with R = Pr, Dy, Tb and Tm) to explain high-field magnetization measurements revealing a field-induced metamagnetic transition for the field along the c axis [8, 9].

Another possibility is that the local susceptibility is modified by the presence of the μ^+ via a change of the CEF splitting of the nearest Ce^{3+} neighbours. Such an effect has been successfully invoked in explaining the loss of the μ^+-Knight shift versus susceptibility scaling in $PrNi_5$ [27], $PrIn_3$ [28], UNi_2Al_3 [29], and $TmNi_2B_2C$ [18]. Corresponding CEF calculations are planned also for the present system. However, it appears rather unlikely that the ordered moments in the vicinity of the μ^+ could be modified, and in fact such a change has never been observed before.

6. Summary

TF, LF and ZF μSR measurements were performed on monocrystalline $CeCu_2$ samples.

As with the isostructural compounds $GdCu_2$ and $PrCu_2$, $CeCu_2$ accommodates the μ^+ at a unique 4e site, the free z co-ordinate of which could be well determined. This was achieved using the measured T dependences of the μ^+ Knight-shift components K_c and K_b (with $\boldsymbol{H} \parallel \boldsymbol{c}$ and $\boldsymbol{H} \parallel \boldsymbol{b}$, respectively), relating them to the corresponding susceptibility components and comparing the outcome to dipolar and contact-hyperfine field calculations for all muon-site candidates.

A T-independent contact-hyperfine coupling constant A_0, arising from the spin polarization of the conduction electrons at the μ^+, is determined at the same time.

With $\boldsymbol{H} \parallel \boldsymbol{b}$ the local magnetic susceptibility χ_b^{loc} (induced by the μ^+ presence) is equivalent to the bulk susceptibility for 14 K $\leqslant T \leqslant$ 300 K, whereas with $\boldsymbol{H} \parallel \boldsymbol{c}$ the local susceptibility, determined by a Curie–Weiss relation fitted to the K_c data for $T \geqslant 70$ K, is very different from χ_c^{bulk}. These features are most probably caused by a μ^+ induced change of the CEF splitting of the nearest Ce^{3+} neighbours and a correspondingly modified local susceptibility.

The relaxations of the LF and TF μSR signals, found to be essentially of dynamical origin, are well described by the Redfield formulae. The fluctuating magnetic field amplitudes at the μ^+ positions are heavily anisotropic, strongest in the c-axis direction, weakest along the a axis. Assuming T-independent fluctuation amplitudes, the relaxations can be characterized above 14 K by two fluctuation rates following Arrhenius laws, one effective below and the other respectively above 100 K. For the temperature range studied, above 5 K, one stays always in a regime of fast fluctuations ($\omega^2\tau_0^2 \ll 1$), i.e., with a fluctuation time τ_0 clearly below 2 ns. The observed field fluctuation pattern cannot be due to a fully random fluctuation of the magnetic Ce moments, but it could be explained if the dominant moment fluctuation amplitude is along the $\boldsymbol{b}$ axis.

Below the Néel temperature, ZF measurements reveal a spontaneous precession frequency $\nu(T)$ corresponding to static magnetic fields of single magnitude (for a given temperature), oriented parallel to the crystallographic $\pm\boldsymbol{c}$ directions at the muon sites. This field pattern is consistent with the known magnetic structure of $CeCu_2$ [6, 7]. Near T_{N} the T dependence of ν follows a $[1 - (T/T_{\mathrm{N}})]^{\beta}$ relation, whereas at low temperature the frequency goes like $\nu_0(1 - AT^{\epsilon})$. One extracts a critical behaviour parameter $\beta = 0.50(1)$, corresponding to a simple mean-field calculation. At low T, where the magnon effects should be visible, one

obtains $\epsilon = 2.6(1)$, somewhat larger than the 2.0 expected from calculations for a *cubic* 3D antiferromagnet.

Temperature dependences inferred from neutron diffraction reflection data [25] seem to behave like the spontaneous μSR frequency. However, the two oriented Ce moment values extracted from n-measurements [7, 25] are not convincingly consistent, and are not compatible with the findings of the present work. Part of the discrepancy could possibly be explained by a change of the contact-hyperfine coupling A_0 at low temperature. However, we suggest considering first an improved neutron data analysis or additional n-scattering measurements.

Acknowledgments

We thank the Laboratory for Muon-Spin Spectroscopy (LMU), in particular C Baines and A Amato, responsible for the LTF and GPS instruments, and the proton accelerator crew of the Paul Scherrer Institut (PSI) for providing excellent measuring conditions.

References

[1] Schenck A, Andreica D, Gygax F N, Pinkpank M, Ōnuki Y, Ahmet P, Abliz M, Settai R, Amato A and Kaplan N 1998 *Phys. Rev.* B **58** 5205
[2] Schenck A, Gygax F N and Ōnuki Y 2003 *Phys. Rev.* B **68** 104422
[3] Gygax F N, Andreica D, Schenck A and Ōnuki Y 2002 *J. Magn. Magn. Mater.* **246** 101
[4] Hillberg M, Wagener W, de Melo M A C, Klauss H H, Litterst F J and Loewenhaupt W 1997 *Hyperfine Interact.* **104** 307
[5] For a general review see Luong N H and Franse J J M 1995 *Magnetic Properties of Rare Earth–Cu_2 Compounds* (*Handbook of Magnetic Materials* vol 8) ed K H J Buschow (Amsterdam: Elsevier) p 415
[6] Trump R, Thierfeldt S, Loewenhaupt M and Chattopadhyay T 1991 *J. Appl. Phys.* **69** 4699
[7] Nunez V, Trump R, Brown P J, Chattopadhyay T, Loewenhaupt M and Tasset F 1992 *J. Phys.: Condens. Matter* **4** 1115
[8] Sugiyama K, Nakashima M, Yoshida Y, Settai R, Takeuchi T, Kindo K and Ōnuki Y 1999 *Physica* B **259** 896
[9] Sugiyama K, Yamamoto T, Nakamura N, Kindo K, Settai R and Ōnuki Y 2003 *J. Magn. Magn. Mater.* **262** 389
[10] Loewenhaupt M, Prager M, Gratz E and Frick B 1988 *J. Magn. Magn. Mater.* **76/77** 415
[11] Loewenhaupt M, Witte U, Kramp S, Braden M and Svoboda P 2002 *Physica* B **312/313** 181
[12] Homepage of the Laboratory for Muon Spectroscopy of PSI, http://lmu.web.psi.ch
[13] Satoh K, Fukada A, Umehara I, Ōnuki Y, Sato H and Takayanagi S 1992 *J. Phys. Soc. Japan* **61** 3267
[14] Schenck A and Gygax F N 1995 *Handbook of Magnetic Materials* vol 9, ed K H J Buschow (Amsterdam: Elsevier) p 57
[15] Schenck A 1999 *Muon Science* ed S L Lee, S H Kilcoyne and R Cywinsky (Bristol: SUSSP Publications and Institute of Physics Publishing) p 39
[16] Data from Sugiyama K and Ōnuki Y superseding the susceptibility reported in [13]
[17] Akishin P G and Gaganov I A 1992 *J. Magn. Magn. Mater.* **110** 175
[18] Gygax F N, Schenck A, Solt G and Canfield P C 2003 *Physica* B **326** 359
[19] De Lorenzi F, Gygax F N, Schenck A, Tobo A and Onodera H 2003 *Physica* B **326** 581
[20] Schenck A, Pinkpank M, Gygax F N, Neumann K U, Ziebeck K R A and Amato A 1998 *J. Phys.: Condens. Matter* **10** 8059
[21] Uemura Y J 1999 *Muon Science* ed S L Lee, S H Kilcoyne and R Cywinsky (Bristol: SUSSP Publications and Institute of Physics Publishing) p 85
[22] Slichter C P 1990 *Principles of Magnetic Resonance* (Berlin: Springer)
[23] Hohenemser C, Rosov N and Kleinhammes A 1989 *Hyperfine Interact.* **49** 267
[24] Kubo R 1952 *Phys. Rev.* **87** 568
[25] Rotter M, Loewenhaupt M and Witte U 1999 *Annual Report* Hahn-Meitner-Institut, Berlin, p 60
[26] Schenck A, Gygax F N, Andreica D and Ōnuki Y 2003 *J. Phys.: Condens. Matter* **15** 8599
[27] Feyerherm R, Amato A, Grayevsky A, Gygax F N, Kaplan N and Schenck A 1995 *Z. Phys.* B **99** 3
[28] Tashma T, Amato A, Grayevsky A, Gygax F N, Pinkpank M, Schenck A and Kaplan N 1997 *Phys. Rev.* B **56** 9397
[29] Schenck A, Sato N K, Solt G, Andreica D, Gygax F N, Pinkpank M and Amato A 2000 *Eur. Phys. J.* B **13** 245